Journal of Alloys and Compounds 702 (2017) 146–152

Contents lists available at ScienceDirect

Journal of Alloys and Compounds

journal homepage: http://www.elsevier.com/locate/jalcom

Peptide capped Pd nanoparticles for oxygen electroreduction: Strong surface effects

Hongyu Yang [a], Zhenghua Tang [a, b, *], Wei Yan [a], Likai Wang [a], Qiannan Wang [a], Yongqing Zhang [b], Zhen Liu [c, d], Shaowei Chen [a, e, **]

[a] New Energy Research Institute, School of Environment and Energy, South China University of Technology, Guangzhou Higher Education Mega Centre, Guangzhou, 510006, China
[b] Guangdong Provincial Key Laboratory of Atmospheric Environment and Pollution Control, Guangdong Provincial Engineering and Technology Research Center for Environmental Risk Prevention and Emergency Disposal, South China University of Technology, Guangzhou Higher Education Mega Centre, Guangzhou, 510006, China
[c] Department of Materials Science and Engineering, University of Maryland, College Park, MD, 20742-4111, United States
[d] Department of Physics & Engineering, Frostburg State University, Frostburg, MD, 21532-2303, United States
[e] Department of Chemistry and Biochemistry, University of California, 1156 High Street, Santa Cruz, CA, 95064, United States

ARTICLE INFO

Article history:
Received 15 October 2016
Received in revised form
16 January 2017
Accepted 19 January 2017
Available online 23 January 2017

Keywords:
Peptide
Palladium nanoparticles
Fuel cell
Electrocatalyst
Oxygen electroreduction
Surface effects

ABSTRACT

Peptide-capped nanoparticles represent a unique type of nanomaterials with emergent optical and electrochemical properties. Herein, a series of peptide capped palladium nanoparticles have been prepared and employed as highly efficient catalysts for oxygen electroreduction. The peptide sequence was tuned by substituting amino acid residues at specialized positions, and strong surface effects were observed between the peptide sequence and the electrocatalytic activity. The findings corresponded well with the previously reported C–C coupling catalytic reactions, indicating that the residue-specific binding effects but not the overall binding strength governed the electrocatalytic activity. The results may shed light on the rational design of bio-inspired nanomaterials with optimized electrocatalytic properties.

1. Introduction

Bio-mimetics represent new avenues to the fabrication of functional nanomaterials that can find technologically important applications such as catalysis [1,2], plasmonics [3], assembly [4,5], energy storage and conversion [6,7], as well as biomedical diagnostics and therapeutics [8]. By introducing biological specificity into nanomaterial synthesis, controllable size, shape and composition with desirable functionalities can be achieved. Biomolecules such as DNA, protein and peptide (e. g., peptide sequences with specific binding affinity to inorganic substrates such as Pt [9,10], Au [11], Ag [12], TiO_2 [13], and SiO_2 [14]) have been widely employed as templates to guide the preparation of various nanostructures [15,16]. Whereas remarkable progress has been made, the effects of the biotic/abiotic interface on the materials properties remain largely elusive. For example, peptide capped noble metal nanoparticles have been employed as efficient catalysts in various reactions, the correlation between the peptide sequence and the structure/function of the as-formed nanomaterials still has not been established, except for a few successful examples [17–19].

Thanks to their extraordinary catalytic performance, palladium nanoparticles (PdNPs) have been attracting extensive attentions in recent decades [20–23]. To fabricate stable and reactive PdNPs, peptides with specific binding affinity were introduced to prevent the aggregation and/or decomposition. Pd4 (TSNAVHPTLRHL), one of the Pd binding sequence, was first isolated by a phage display technique [24]. Knecht group reported the facile fabrication of Pd4 capped PdNPs and found that they possessed an extraordinary

* Corresponding author. New Energy Research Institute, School of Environment and Energy, South China University of Technology, Guangzhou Higher Education Mega Centre, Guangzhou, 510006, China.
** Corresponding author. New Energy Research Institute, School of Environment and Energy, South China University of Technology, Guangzhou Higher Education Mega Centre, Guangzhou, 510006, China.
E-mail addresses: zhht@scut.edu.cn (Z. Tang), shaowei@ucsc.edu (S. Chen).

http://dx.doi.org/10.1016/j.jallcom.2017.01.199
0925-8388/

catalytic activity for C–C coupling reactions with a high yield under environmental friendly conditions (with water as the solvent and at room temperature) [25,26]. With the combination of experimental results and computational calculations, the histidine residues at the 6th and 11th positions were found to act as the anchors for the Pd4 sequence to bind on the metallic surface [27]. When the two histidine groups were substituted by other amino acids to vary the binding strength, the corresponding peptide capped PdNPs exhibited different catalytic activity for the C–C coupling reactions [28]. This suggests peptide surface effects on the catalytic performance. Peptide-assembled materials have been employed for solar energy storage and conversion and other energy related applications [29–31], while peptide assisted/based noble metal nanoparticles have been reported as catalysts for electrochemical processes. For instance, Wang et al. demonstrated the fabrication of highly active and stable Pt(111)-P/C catalyst for oxygen electroreduction with the assistance of peptide [32]. Recently, Bedford and coworkers showcased the surface segregation of peptide directed AuPd bimetallic nanoparticles, and surface-dependent catalytic activities were observed for methanol oxidation [33]. However, how the peptide sequence affects the electrochemical catalytic activity and the correlation between the peptide sequence and electro-catalytic performance of the as-formed peptide capped nanoparticles still remain unclear. This is the primary motivation of the present study, where the effects of peptide sequences on the electrocatalytic activity of PdNPs towards oxygen reduction reaction (ORR) were examined. ORR is a key step that limits the widespread commercialization of low temperature fuel cells, and the most commonly used electrode catalysts are based on platinum which suffer from the scarcity and high price of Pt [34–36]. Bio-inspired nanocatalysts can significantly lower the costs of the electrode materials whilst providing remarkable activity and long-term stability. Unfortunately, examples have been rare to date [37–39]. Recently, Kim group reported the fabrication and catalytic response to oxygen electroreduction of surface-composition-controlled AuPt bimetallic nanoparticles on carbon nanotubes [40]. Our group also reported the fabrication of peptide R5 templated Au and Pt nanomaterials for ORR, where the shape/morphology of the metal nanomaterials played an important role in the electrocatalytic performance [41].

Herein, a series of peptide capped PdNPs were fabricated and used as highly efficient catalysts for ORR. Pd4 peptide was used as the parent sequence where the histidine residues at the 6th and 11th positions were substituted by cysteine and alanine residues. Among twenty natural amino acids, cysteine, histidine and alanine have been known to exhibit the strongest, the intermediate and the weakest binding affinity to palladium surfaces [42]. Thus, cysteine and alanine are selected to substitute histidine to tune the binding strength of the Pd4 sequence. Experimentally, six peptide sequences were prepared (Table S1) and the Gibbs free energy of these six peptides binding to palladium surfaces has been quantified by quartz crystal microbalance (QCM) measurements previously [28]. The corresponding peptide-capped PdNPs demonstrated excellent catalytic activity toward ORR. However, the performance varies drastically with the peptide sequence. The results suggest that the electrocatalytic performance were probably dictated by the specific binding residues in the sequence but not the overall peptide binding strength.

2. Materials and methods

2.1. Chemicals

Peptide Pd4 (TSNAVHPTLRHL, >96%), C6 (TSNAVCPTLRHL, >96%), C11 (TSNAVHPTLRCL, >96%), C6, 11 (TSNAVCPTLRCL, >96%), A6C11 (TSNAVAPTLRCL, >96%), C6A11 (TSNAVCPTLRAL, >96%) were purchased from Top-Peptide (Shanghai, China). Potassium tetrachloropalladate (K_2PdCl_4, 98%) and sodium borohydride ($NaBH_4$, 98%) were acquired from Aladdin Industrial Corporation (Shanghai, China). Polyvinylpyrrolidone (PVP, MW: 8000), glutathione (98%), Pt/C and Pd/C were purchased from Energy Chemicals (Shanghai, China). Water was supplied by a Barnstead Nanopure Water System (18.3 MΩ cm).

2.2. Synthesis of peptide capped palladium nanoparticles (PdNPs)

Peptide capped PdNPs were synthesized by the following a modified procedure in the previous reports. Briefly, 2 mg peptide (Pd4, C6, C11, C6,11, A6C11 or C6A11) was first dissolved in 0.775 mL of purified water in a 10 mL beaker at room temperature. 0.137 mL of 38.43 mM K_2PdCl_4 was then added into the above solution. After the mixture was incubated for 30 min, 1.088 mL of freshly prepared 0.02 M $NaBH_4$ solution was added rapidly where the color of solution turned from colorless to brown immediately. Then the solution was kept incubating for at least 1 h. The peptide capped PdNPs were obtained.

2.3. Characterizations

UV–visible absorption of the peptide capped PdNPs was measured using a Shimadzu 2600/2700 UV–visible scanning spectrophotometer with a 1 cm quartz cuvette. TEM images were acquired with high-resolution transmission electron microscope (JEOL-JEM-2010), where samples were prepared by dropcasting a catalyst dispersion directly onto a copper grid coated with a holey carbon film. CD analysis was operated on a Chirascan CD spectrometer (Applied Photophysics, UK).

2.4. Electrochemical measurements

Electrochemical measurements were performed with a CHI 750E electrochemical workstation (CH Instruments Inc.) in a 0.1 M KOH aqueous solution at room temperature. A platinum wire and a Ag/AgCl electrode were employed as the counter electrode and reference electrode, respectively. The Ag/AgCl reference electrode was calibrated with respect to a reversible hydrogen electrode (RHE) by the formula of $E_{Ag/AgCl} = E_{RHE} + 0.96\ V$ in all measurement. The working electrode was a ring-disk electrode (diameter 5.61 mm) and cleaned by mechanical polishing with aqueous slurries of 0.3 μm alumina powders on a polishing microcloth. The samples was prepared by dropping 10 μL PdNPs aqueous solution and 1 μL Nafion (5 wt%, Aldrich) on the glassy carbon disk of the working electrode and dried at room temperature. The catalyst loading was ~80 $\mu g/cm^2$ for the six samples.

3. Results and discussion

3.1. HR-TEM images of the six type of peptide capped PdNPs

PdNPs capped by the six sequences were synthesized by a facile wet chemical approach (see experimental details in Supporting information). Fig S1 presents the UV–visible absorption spectra of these PdNPs. All the solutions exhibited a dark brown color and a nearly identical featureless, exponential decay profile, consistent with palladium colloids [43]. The size and morphology of the as-prepared PdNPs were then examined by high resolution transmission electron microscopy (HRTEM), and representative images are depicted in Fig. 1. It can be seen that the PdNPs were all evenly dispersed without apparent aggregation. Based on statistical analysis of more than 200 nanoparticles, the average core diameters of

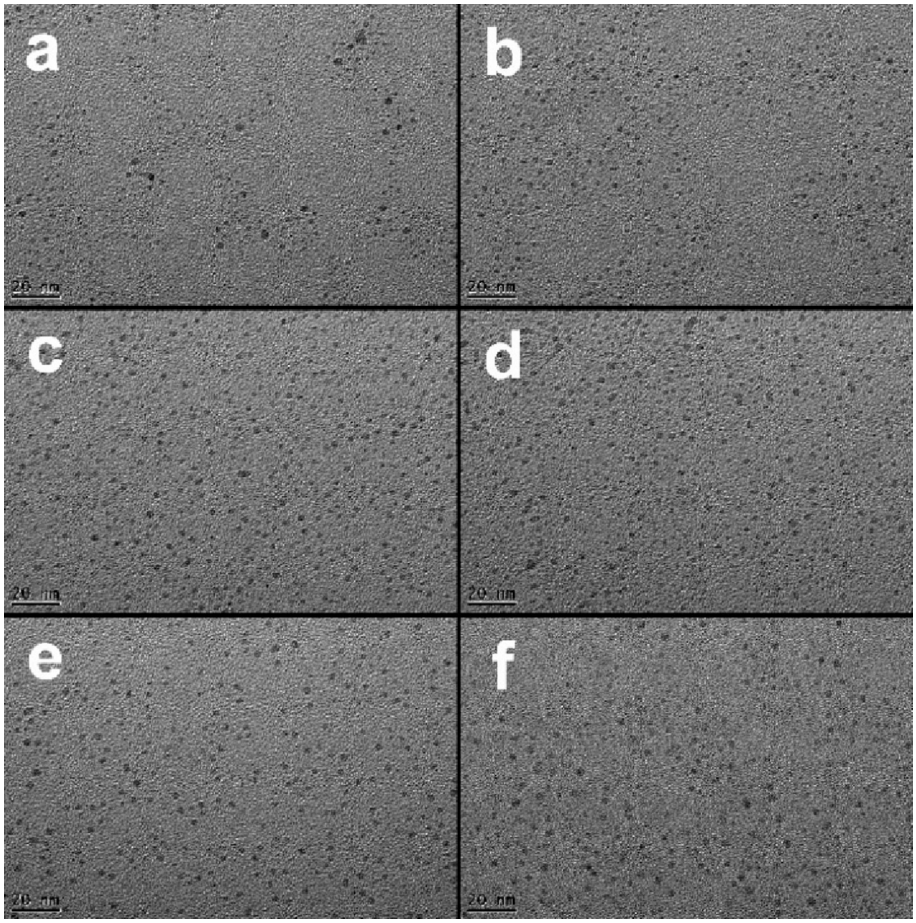

Fig. 1. Representative HR-TEM images of (a) Pd4-PdNPs, (b) C6-PdNPs, (c) C11-PdNPs, (d) C6,11-PdNPs, (e) A6C11-PdNPs and (f) C6A11-PdNPs. Scale bars all 20 nm. The corresponding size distribution histograms are included in Fig S2.

the PdNPs are estimated to be around 1.8 nm (Table S1), with the corresponding core size histograms presented in Fig S2. One can see that the average core diameter is 1.7 ± 0.5 nm for Pd4-PdNPs, 1.8 ± 0.4 nm for C6-PdNPs, 1.8 ± 0.3 nm for C11-PdNPs, 1.8 ± 0.4 nm for C6,11-PdNPs, 2.0 ± 0.4 nm for A6C11-PdNPs and 1.9 ± 0.4 nm for C6A11-PdNPs. It is worth noting that for the particles prepared with cysteine-substituted peptides (C6, C11, and C6,11), the sizes are basically identical to that of Pd4-PdNPs; while for particles capped by C6A11 or A6C11 peptides, a slight difference was observed, where the core dimensions are larger than those of the other four nanoparticles. One may notice that there is no clear correlation between the nanoparticle size and the peptide binding strength. The results suggest that the nanoparticle size is more relevant with the interaction of individual amino acid residues with the palladium surface rather than with the overall binding affinity of the peptide sequence [26]. In fact, it has been recorded that the size of these peptide-capped metal nanoparticles can be controlled by the peptide binding motif but not by the total binding strength [11,12,44]. Additionally, from high-resolution TEM studies (Fig S3), one can see well-defined crystalline lattice fringes of the nanoparticles, where the interplanar distance of 0.23 nm is consistent with the Pd(111) planes [45–47].

In addition, X-ray photoelectron spectroscopy (XPS) was conducted to examine the electronic state of all the peptide capped Pd NPs. The survey scan spectra confirmed the presence of Pd, N, C and O (Fig S4). As shown in Fig S5, for all the samples, the Pd3d spectra can be de-convoluted into two doublets. The pair at lower binding energies (334.0 eV and 340.4 eV) correspond with metallic Pd, whereas those at somewhat higher binding energies (336 eV and 341.5 eV) can be ascribed to Pd(II) species [48,49].

3.2. CD analysis of the six peptide capped PdNPs

Next, the peptide conformation before and after binding to PdNPs were studied. As shown in Fig. 2, for the peptide ligands, A6C11 and C11 display higher ellipticity than C6, C6A11 and C6,11, all higher than Pd4. After binding on palladium, the ellipticities of A6C11, C11, C6, C6A11, C6,11 and Pd4 were −26.4, −28.8, −19.7, −21.0, −20.4 and −13.4, respectively, in the same trend before binding. However, upon binding onto PdNPs, peptides C6, C6,11 and C6A11 exhibited a large decrease in ellipticity at ~199 nm, as compared to the free peptides (51.9% for C6, 45.9% for C6,11, and 47.0% for C6A11). As for C11, A6C11 and Pd4, such decrease were 41.6%, 41.7% and 43.4%, respectively. The results indicate that in the presence of cysteine at the 6th or 11th position, the peptide adopt an increasingly disordered structure. One can conclude that the total peptide surface structure would be more affected by cysteine substitution at the 6th position than 11th position due to the amino acid residue pinning at the centre of the sequence.

It is interesting to notice that the Pd-bound C6, C6,11 and C6A11 possessed similar CD spectra, while the Pd-bound C11 and A6C11 possessed similar CD spectra. For C11 and A6C11, the dominant negative peak shifted from 198 nm to 203 nm upon palladium

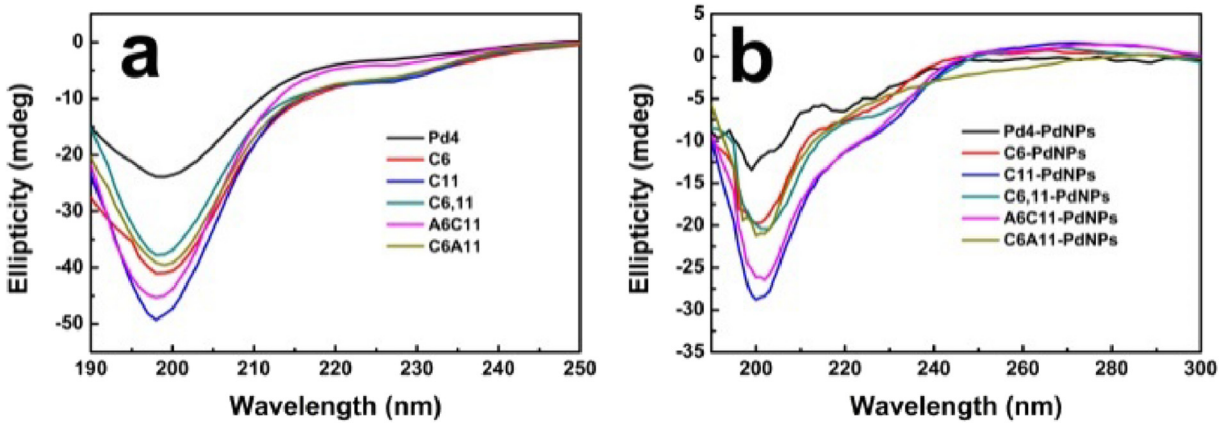

Fig. 2. CD analysis of the peptides (a) before and (b) after binding to the PdNPs. The measurements were conducted with a nanoparticle concentration of 0.2 g/L.

binding and a shoulder appeared at 235 nm. The spectra displayed partial characteristic feature of a polyproline type II helix, which corresponds with a structural assignment of a 9-mer polyproline peptide documented before [50]. Note that, compared with other sequences, Pd-bounded A6C11 and C11 peptides both possess higher ellipticity, suggesting a more compact surface structure, while the Pd-bound A6C11 peptide has a decreased ellipticity than C11, indicating the sequence A6C11 is more unfolded on the palladium surface. Furthermore, the as-prepared PdNPs capped with the peptides of C6, C6A11 and C6,11 exhibited similar ORR activity, while PdNPs capped by the peptides of A6C11 and C11 exhibited larger but also similar ORR activity, which will be discussed next.

3.3. Electrocatalytic measurements toward ORR of the as-prepared PdNPs

The electrocatalytic activity toward ORR of the as-prepared PdNPs was first investigated and compared with voltammetric measurements. As presented in Fig. S6, only featureless charging current was observed in N_2-saturated 0.1 M KOH in the potential range of −0.04 V to +1.16 V in each sample. However, when the solution was saturated with oxygen, a cathodic current peak attributed to oxygen reduction can be clearly identified. The cyclic voltammograms of a glassy carbon electrode modified with the six peptide capped PdNPs were shown in Fig. 3. The cathodic peak potentials were estimated to be +0.58 V for Pd4-PdNPs, +0.68 V for C6-PdNPs, +0.76 V for C11-PdNPs, +0.62 V for C6,11-PdNPs, +0.74 V for A6C11-PdNPs and +0.63 V for C6A11-PdNPs. One can see that C11-PdNPs and A6C11-PdNPs possess very close but more positive cathodic peak potentials than C6-, C6A11-and C6,11-PdNPs, which are more positive than that of Pd4-PdNPs. Moreover, high cathodic peak current densities from C11-PdNPs (−0.38 mA·cm^{-2}) and A6C11-PdNPs (−0.39 mA·cm^{-2}) were also observed. However, the peak current densities of C6-PdNPs, C6,11-PdNPs, C6A11-PdNPs and Pd4-PdNPs were extremely close, which were in the range from −0.31 to −0.34 mA·cm^{-2}. The results suggest that A6C11-PdNPs and C11-PdNPs possess the best activity among the series of samples, followed by C6-, C6,11-, and C6A11-PdNPs, whereas the Pd4-PdNPs exhibit the lowest activity.

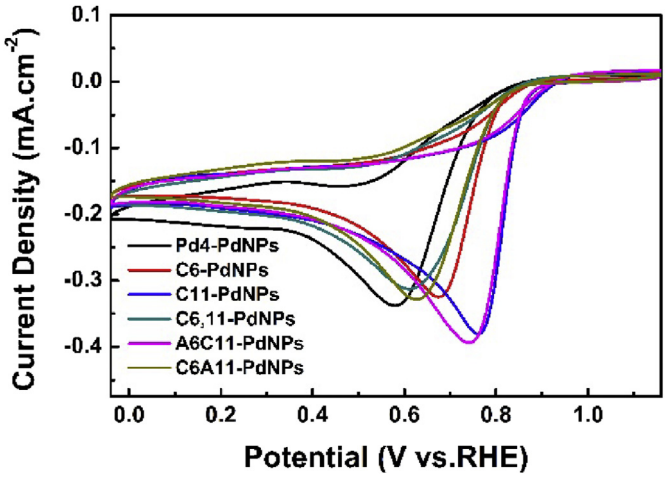

Fig. 3. Cyclic voltammograms of a glassy carbon electrode modified with the six peptide capped PdNPs in O_2-saturated 0.1 M KOH. Potential scan rate is 10 mV s^{-1}.

The effects of peptide sequence on ORR activity were further probed in rotating ring-disk electrode (RRDE) voltammetric measurements, as depicted in Fig. 4a [51]. Interestingly, the onset potential and current density of these PdNPs vary drastically with the peptide sequence. C11-PdNPs and A6C11-PdNPs possess an almost identical onset potential at +0.89 V, which is the most positive among the series. For C6-, C6,11-, and C6A11-PdNPs, the onset potentials were very close at +0.85 V, +0.85 V and +0.83 V, respectively. Pd4-PdNPs possess the least positive onset potential at +0.81 V. The results were consistent with those from the cyclic voltammetric measurements (Fig S6). In addition, although C11-PdNPs and A6C11-PdNPs possess a close cathodic peak potential and onset potential, the diffusion limited current density (at +0.50 V and 1600 rpm) is quite different, −2.82 mA·cm^{-2} for C11-PdNPs and −3.36 mA·cm^{-2} for A6C11-PdNPs. From these observations, it seems that A6C11-PdNPs bear slightly better activity than C11-PdNPs. LSV curve of this two PdNPs at various rotating rates of 100–2500 rpm are shown in Fig S7. In comparison, the diffusion limited current density of C6-, C6A11-and C6,11-PdNPs is quite close, while Pd4-PdNPs possess the lowest value among the series of samples. Therefore, one can conclude that for the six peptide-capped PdNPs, the catalytic activity for ORR decreases in the order of C11-, A6C11- PdNPs > C6-, C6,11- and C6A11-PdNPs > Pd4-PdNPs. A6C11- and C11-PdNPs exhibited the best electrocatalytic activity and A6C11-PdNPs outperform C11-PdNPs slightly. Compared with other widely employed stabilizing agents such as Glutathione and polyvinyl pyrrolidone (abbreviated as PVP), peptides exhibit greater superiority. A comparison measurement was conducted between C11, A6C11-PdNPs and PVP- as well as Glutathione-PdNPs. As depicted in Fig. 4b, The onset potential of PVP-Pd NPs and Glutathione-PdNPs was 0.81 V and 0.69 V,

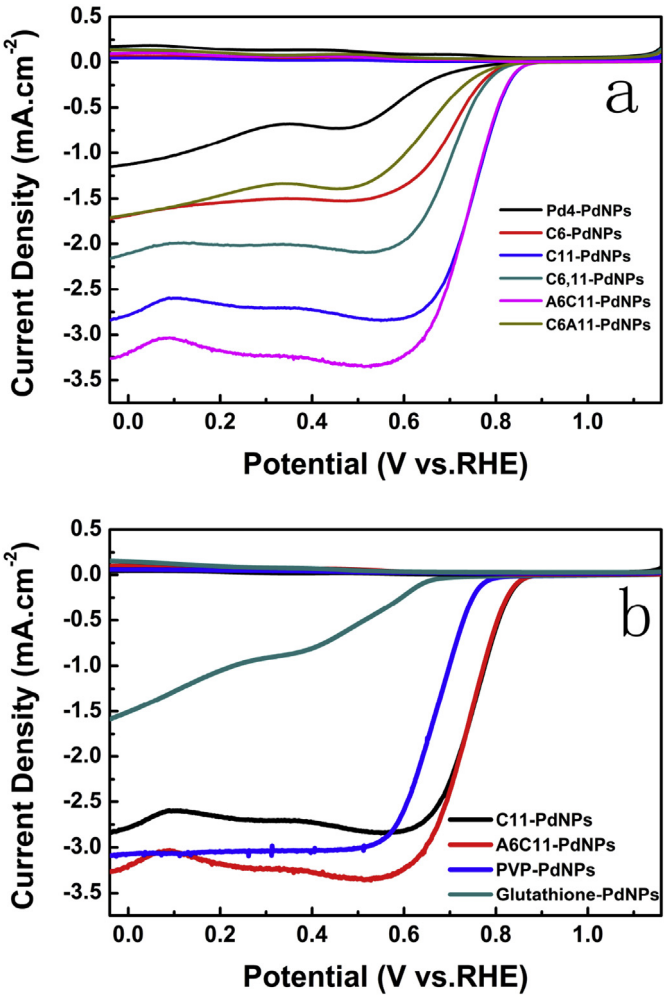

Fig. 4. (a) RRDE voltammograms of a glassy carbon electrode modified with the six peptide capped PdNPs and (b) Comparison of RRDE voltammograms with PVP- and Glutathione-PdNPs in O_2-saturated 0.1 M KOH. Potential scan rate 10 mV s^{-1}, and rotation rate is 1600 RPM.

respectively, much lower than that of C11, A6C11-PdNPs, indicating an inferior activity.

Based on the RRDE measurements (Fig. 4), the number of electron transfer (n) and H_2O_2 yield in ORR can be quantified by

$$n = \frac{4I_d}{I_d + I_r/N}$$

and

$$H_2O_2\% = \frac{200I_r/N}{I_r/N + I_d}$$

where I_d is disk current density, I_r is ring current density, and N is the RRDE collection efficiency (0.37). Within the potential range of −0.04 V to +0.6 V, the numbers of electron transfer (n) are 3.23–3.56 for Pd4-PdNPs, 3.45–3.59 for C6-PdNPs, 3.73–3.87 for C11-PdNPs, 3.73–3.85 for C6,11-PdNPs, 3.77–3.91 for A6C11-PdNPs, 3.50–3.74 for C6A11-PdNPs and 3.78–3.94 for Pt/C (Fig S8). The number of electron transfer follows the same trend of A6C11-, C11- PdNPs > C6-, C6,11- and C6A11- PdNPs > Pd4-PdNPs, and for C11- and A6C11- PdNPs, the N values are quite close to that of Pt/C (3.79–3.93), but higher than that of Pd/C (3.64–3.91). Similarly, the H_2O_2 yield is less than 40% for all peptide capped PdNPs (Fig S8); For C11- and A6C11-PdNPs, the yields are 6.86–14.76% and 4.83–12.99% respectively, which are comparable to that of Pt/C (3.35–10.96%) and lower than that of Pd/C (4.79–18.86%). With the combined results, we can conclude that C11- and A6C11- PdNPs possessed higher electrocatalytic activity toward ORR comparable with Pt/C but superior than Pd/C. Furthermore, the corresponding Koutecky-Levich (K-L) plots for C11- and A6C11-PdNPs at different electrode potentials are presented in Fig S9. In the potential range of +0.59 V - +0.77 V, a good linearity with a consistent slope was obtained, which implies first order reaction kinetics of ORR with respect to oxygen concentration in the solution.

A clear trend for ORR was noted within the context of the peptide sequence. With a strong binder at the 11th position and a weak binder at the 6th position (C11, A6C11), the modified sequence capped PdNPs possess higher catalytic activity than the sequences with the 6th position modified by a strong binder (C6, C6,11 and C6A11). In addition, PdNPs capped by the native peptide Pd4 demonstrated the lowest ORR activity among the series of samples.

3.4. Mechanistic study and ORR activity analysis

In previous studies of oxygen electroreduction on Pd in alkaline media, the reaction mechanism was found to be similar with that on Pt [52]. The key steps can be summarized below:

$$O_2 + * + e \rightarrow O_2^{-*} \quad (a)$$

$$O_2^{-*} + H_2O \rightarrow HO_2^{*} + OH^{-} \quad (b)$$

$$HO_2^{*} + e \rightarrow HO_2^{-*} \quad (c)$$

$$HO_2^{-*} + e \rightarrow H_2O + e \rightarrow OH^{*} + 2OH^{-} \quad (d)$$

$$OH^{*} + e \rightarrow OH^{-} + * \quad (e)$$

where asterisks denote surface-adsorbed species. Among these, the first electron reduction of O_2^* to HO_2^* is the rate-determining step (a and b), and the subsequent step (d) involves the breaking of the O–O bond. It is worth noting that if the adsorption of O_2 on the catalyst surface is too weak, the breaking of O–O bond will be slow.

In the present study, the metal core surface structure of the PdNPs is pivotal for the adsorption of oxygen molecules, which probably dominate the ORR activity. It is well known that thiols have strong binding interaction on noble metal surface, which can lead to diminished activity due to the thiol poisoning effects [53,54]. For C11 and A6C11, the histidine at the 11th position was replaced by cysteine which has a thiol group. As shown in Scheme 1, a clear trend for ORR was noted within the context of the peptide sequence. On the surface of C11- and A6C11-PdNPs, it is likely that the strong binding from cysteine near the terminal (the 11th position) of the sequence “releases” other amino acid residues, which allows the maximal access for O_2 adsorption. This assumption of offsetting effects actually can be evidenced by the CD results. Note that, after binding to Pd surface, the as-formed C11- and A6C11-PdNPs possessed larger ellipticity in the series, indicating both of them bear a more disordered surface structure. Furthermore, such offsetting effects are not so strong for C6-, C6,11- and C6A11- PdNPs, as the strong binding from cysteine is in the middle of the sequence (the 6th position).

Nevertheless, recent combinational studies from the pair distribution function analysis and molecular dynamic simulations

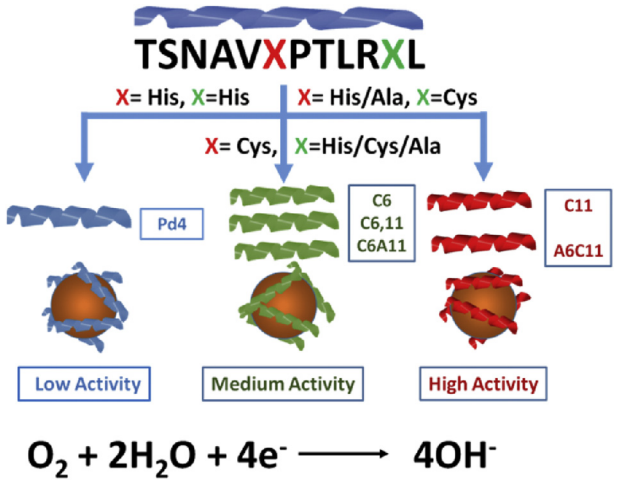

Scheme 1. Effects of peptide sequence of peptide capped PdNPs for ORR.

demonstrated that a minor change of the peptide sequence might cause significant variation of the highly disordered surface atoms [18]. Note that how these highly disordered surface atoms influence the catalytic activity varies differently from different catalytic reaction [18]. Yet, structural comprehension on the atomic level still remains elusive for electrocatalytic reactions, and further research efforts on computational calculation are probably needed.

3.5. *Long-term durability tests compared with commercial Pt/C and Pd/C*

Finally, the durability of A6C11- and C11- PdNPs with commercial Pt/C and Pd/C was compared and evaluated by chronoamperometric measurements [55]. As depicted in Fig. 5, after 8 h 's continuous operation, the cathodic currents of commercial Pt/C and Pd/C catalysts displayed a loss of ~34% and ~32% of the initial value, while for A6C11- and C11-PdNPs, the loss is only 18.1% and 14.6%, respectively. Both PdNPs exhibited remarkable stability markedly better than commercial Pt/C and Pd/C catalysts, and the ORR performance of C11, A6C11-PdNPs was virtually invariant when the samples were recycled and tested 3 times (Fig S10).

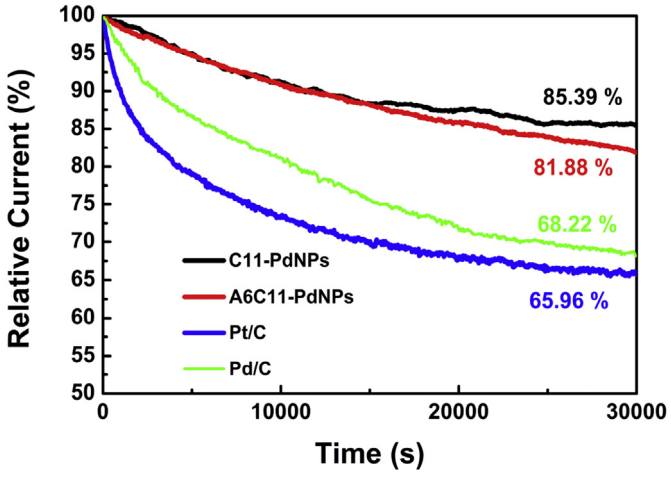

Fig. 5. Chronoamperometric responses for ORR at C11-PdNPs, A6C11-PdNPs, Pt/C and Pd/C electrodes in an O_2-saturated 0.1 M KOH solution for 30 000 s.

4. Conclusions

In summary, a series of peptide capped PdNPs have been employed as highly efficient catalyst for oxygen electroreduction. All the peptide capped PdNPs demonstrated highly efficient reactivity upon ORR, and strong surface effects have been established between the peptide sequence and the catalytic activity on ORR. The ORR activity follow in an order of C11-, A6C11- PdNPs > C6-, C6,11- and C6A11- PdNPs > Pd4-PdNPs. A6C11-, C11-PdNPs exhibited highest catalytic activity in the series of sample, in terms of cathodic peak potential, onset potential and stability. The long-term durability of A6C11-, C11-PdNPs is markedly higher than that of Pt/C as well as Pd/C. The findings here indicate that the residue-specific binding effects but not the overall binding strength governed the electrocatalytic activity. The results can shed light on the rational design of bio-inspired nanomaterials with optimized properties as electrocatalyst. Investigation on further unravelling the electrocatalytic mechanism regarding the different catalytic performance is still underway.

Acknowledgements

Z. H. T acknowledges financial support from Project of Public Interest Research and Capacity Building of Guangdong Province (2015A010105009), Guangdong Innovative and Entrepreneurial Research Team Program (No. 2014ZT05N200), Guangdong Natural Science Funds for Distinguished Young Scholars (No. 2015A030306006) and the National Natural Science Foundation of China (No. 21501059). S.W.C. thanks the National Science Foundation for partial support of the work (CHE-1265635 and DMR-1409396).

Appendix A. Supplementary data

Supplementary data related to this article can be found at http://dx.doi.org/10.1016/j.jallcom.2017.01.199.

References

[1] B.D. Briggs, M.R. Knecht, Nanotechnology meets biology: peptide-based methods for the fabrication of functional materials, J. Phys. Chem. Lett. 3 (2012) 405–418.
[2] R. Bhandari, R. Coppage, M.R. Knecht, Mimicking nature's strategies for the design of nanocatalysts, Catal. Sci. Technol. 2 (2012) 256–266.
[3] L. Tian, J. Luan, K.-K. Liu, Q. Jiang, S. Tadepalli, M.K. Gupta, R.R. Naik, S. Singamaneni, Plasmonic biofoam: a versatile optically active material, Nano Lett. 16 (2016) 609–616.
[4] B.J. Hong, I. Eryazici, R. Bleher, R.V. Thaner, C.A. Mirkin, S.T. Nguyen, Directed assembly of nucleic acid-based polymeric nanoparticles from molecular tetravalent cores, J. Am. Chem. Soc. 137 (2015) 8184–8191.
[5] R. Schreiber, J. Do, E.-M. Roller, T. Zhang, V.J. Schuller, P.C. Nickels, J. Feldmann, T. Liedl, Hierarchical assembly of metal nanoparticles, quantum dots and organic dyes using DNA origami scaffolds, Nat. Nanotechnol. 9 (2014) 74–78.
[6] Y. Lee, J. Kim, D.S. Yun, Y.S. Nam, Y. Shao-Horn, A.M. Belcher, Virus-templated Au and Au-Pt core-shell nanowires and their electrocatalytic activities for fuel cell applications, Energy Environ. Sci. 5 (2012) 8328–8334.
[7] K.T. Nam, D.W. Kim, P.J. Yoo, C.Y. Chiang, N. Meethong, P.T. Hammond, Y.M. Chiang, A.M. Belcher, Virus-enabled synthesis and assembly of nanowires for lithium ion battery electrodes, Science 312 (2006) 885–888.
[8] A.B. Chinen, C.M. Guan, J.R. Ferrer, S.N. Barnaby, T.J. Merkel, C.A. Mirkin, Nanoparticle probes for the detection of cancer biomarkers, cells, and tissues by fluorescence, Chem. Rev. 115 (2015) 10530–10574.
[9] Y. Li, G.P. Whyburn, Y. Huang, Specific peptide regulated synthesis of ultrasmall platinum nanocrystals, J. Am. Chem. Soc. 131 (2009) 15998–15999.
[10] Y. Li, Y. Huang, Morphology-controlled synthesis of platinum nanocrystals with specific peptides, Adv. Mater 22 (2010) 1921–1925.
[11] Z. Tang, J.P. Palafox-Hernandez, W.-C. Law, Z.E. Hughes, M.T. Swihart, P.N. Prasad, M.R. Knecht, T.R. Walsh, Biomolecular recognition principles for bionanocombinatorics: an integrated approach to elucidate enthalpic and entropic factors, ACS Nano 7 (2013) 9632–9646.
[12] J.P. Palafox-Hernandez, Z. Tang, Z.E. Hughes, Y. Li, M.T. Swihart, P.N. Prasad, T.R. Walsh, M.R. Knecht, Comparative study of materials-binding peptide interactions with gold and silver surfaces and nanostructures: a thermodynamic

basis for biological selectivity of inorganic materials, Chem. Mater 26 (2014) 4960–4969.
[13] A. Vallee, V. Humblot, C.-M. Pradier, Peptide interactions with metal and oxide surfaces, Acc. Chem. Res. 43 (2010) 1297–1306.
[14] S.V. Patwardhan, F.S. Emami, R.J. Berry, S.E. Jones, R.R. Naik, O. Deschaume, H. Heinz, C.C. Perry, Chemistry of aqueous silica nanoparticle surfaces and the mechanism of selective peptide adsorption, J. Am. Chem. Soc. 134 (2012) 6244–6256.
[15] M.B. Dickerson, K.H. Sandhage, R.R. Naik, Protein- and peptide-directed syntheses of inorganic materials, Chem. Rev. 108 (2008) 4935–4978.
[16] C.-L. Chen, N.L. Rosi, Peptide-based methods for the preparation of nanostructured inorganic materials, Angew. Chem. Int. Ed. 49 (2010) 1924–1942.
[17] Y. Li, Z. Tang, P.N. Prasad, M.R. Knecht, M.T. Swihart, Peptide-mediated synthesis of gold nanoparticles: effects of peptide sequence and nature of binding on physicochemical properties, Nanoscale 6 (2014) 3165–3172.
[18] N.A. Merrill, E.M. McKee, K.C. Merino, L.F. Drummy, S. Lee, B. Reinhart, Y. Ren, A.I. Frenkel, R.R. Naik, N.M. Bedford, M.R. Knecht, Identifying the atomic-level effects of metal composition on the structure and catalytic activity of peptide-templated materials, ACS Nano 9 (2015) 11968–11979.
[19] N.M. Bedford, Z.E. Hughes, Z. Tang, Y. Li, B.D. Briggs, Y. Ren, M.T. Swihart, V.G. Petkov, R.R. Naik, M.R. Knecht, T.R. Walsh, Sequence-dependent structure/function relationships of catalytic peptide-enabled gold nanoparticles generated under ambient synthetic conditions, J. Am. Chem. Soc. 138 (2016) 540–548.
[20] M.-C. Daniel, D. Astruc, Gold nanoparticles: assembly, supramolecular chemistry, quantum-size-related properties, and applications toward biology, catalysis, and nanotechnology, Chem. Rev. 104 (2004) 293–346.
[21] H. Zhang, M. Jin, Y. Xiong, B. Lim, Y. Xia, Shape-controlled synthesis of Pd nanocrystals and their catalytic applications, Acc. Chem. Res. 46 (2013) 1783–1794.
[22] W. Huang, J.H.-C. Liu, P. Alayoglu, Y. Li, C.A. Witham, C.-K. Tsung, F.D. Toste, G.A. Somorjai, Highly active heterogeneous palladium nanoparticle catalysts for homogeneous electrophilic reactions in solution and the utilization of a continuous flow reactor, J. Am. Chem. Soc. 132 (2010) 16771–16773.
[23] T. Jin, S. Guo, J.-L. Zuo, S. Sun, Synthesis and assembly of Pd nanoparticles on graphene for enhanced electrooxidation of formic acid, Nanoscale 5 (2013) 160–163.
[24] D.B. Pacardo, M. Sethi, S.E. Jones, R.R. Naik, M.R. Knecht, Biomimetic synthesis of Pd nanocatalysts for the stille coupling reaction, ACS Nano 3 (2009) 1288–1296.
[25] R. Coppage, J.M. Slocik, M. Sethi, D.B. Pacardo, R.R. Naik, M.R. Knecht, Elucidation of peptide effects that control the activity of nanoparticles, Angew. Chem. Int. Ed. 49 (2010) 3767–3770.
[26] R. Coppage, J.M. Slocik, B.D. Briggs, A.I. Frenkel, H. Heinz, R.R. Naik, M.R. Knecht, Crystallographic recognition controls peptide binding for bio-based nanomaterials, J. Am. Chem. Soc. 133 (2011) 12346–12349.
[27] R.B. Pandey, H. Heinz, J. Feng, B.L. Farmer, J.M. Slocik, L.F. Drummy, R.R. Naik, Adsorption of peptides (A3, Flg, Pd2, Pd4) on gold and palladium surfaces by a coarse-grained Monte Carlo simulation, Phys. Chem. Chem. Phys. 11 (2009) 1989–2001.
[28] R. Coppage, J.M. Slocik, H. Ramezani-Dakhel, N.M. Bedford, H. Heinz, R.R. Naik, M.R. Knecht, Exploiting localized surface binding effects to enhance the catalytic reactivity of peptide-capped nanoparticles, J. Am. Chem. Soc. 135 (2013) 11048–11054.
[29] E. Gatto, A. Quatela, M. Caruso, R. Tagliaferro, M. De Zotti, F. Formaggio, C. Toniolo, A. Di Carlo, M. Venanzi, Mimicking nature: a novel peptide-based bio-inspired approach for solar energy conversion, ChemPhysChem 15 (2014) 64–68.
[30] Y. Jewel, K. Yoo, J. Liu, P. Dutta, Self-assembled peptides for coating of active sulfur nanoparticles in lithium–sulfur battery, J. Nanoparticle Res. 18 (2016) 54.
[31] V. Nguyen, R. Zhu, K. Jenkins, R. Yang, Self-assembly of diphenylalanine peptide with controlled polarization for power generation, Nat. Commun. 7 (2016) 13566.
[32] W. Wang, Z. Wang, M. Yang, C.-J. Zhong, C.-J. Liu, Highly active and stable Pt (111) catalysts synthesized by peptide assisted room temperature electron reduction for oxygen reduction reaction, Nano Energy 25 (2016) 26–33.
[33] N.M. Bedford, A.R. Showalter, T.J. Woehl, Z.E. Hughes, S. Lee, B. Reinhart, S.P. Ertem, E.B. Coughlin, Y. Ren, T.R. Walsh, B.A. Bunker, Peptide-directed PdAu nanoscale surface segregation: toward controlled bimetallic architecture for catalytic materials, ACS Nano 10 (2016) 8645–8659.
[34] S. Guo, S. Zhang, S. Sun, Tuning nanoparticle catalysis for the oxygen reduction reaction, Angew. Chem. Int. Ed. 52 (2013) 8526–8544.
[35] A. Kraytsberg, Y. Ein-Eli, Review of advanced materials for proton exchange membrane fuel cells, Energy Fuels. 28 (2014) 7303–7330.
[36] Y. Jiao, Y. Zheng, M. Jaroniec, S.Z. Qiao, Design of Electrocatalysts for oxygen- and hydrogen-involving energy conversion reactions, Chem. Soc. Rev. 44 (2015) 2060–2086.
[37] D. Grumelli, B. Wurster, S. Stepanow, K. Kern, Bio-inspired nanocatalysts for the oxygen reduction reaction, Nat. Commun. 4 (2013) 2904–2909.
[38] P.-J. Wei, G.-Q. Yu, Y. Naruta, J.-G. Liu, Covalent grafting of carbon nanotubes with a biomimetic heme model compound to enhance oxygen reduction reactions, Angew. Chem. Int. Ed. 53 (2014) 6659–6663.
[39] B. Zhou, Z. Sun, D. Li, T. Zhang, L. Deng, Y.-N. Liu, Platinum nanostructures via self-assembly of an amyloid-like peptide: a novel electrocatalyst for the oxygen reduction, Nanoscale 5 (2013) 2669–2673.
[40] Y.-S. Ko, Y.-T. Kim, J.-H. Kim, D.H. Kim, K.-H. Kim, W.S. Yun, Y.D. Kim, J. Lee, Y.H. Kim, Peptide-based bimetallic nanostructures with tailored surface compositions and their oxygen electroreduction activities, CrystEngComm 18 (2016) 6024–6028.
[41] Q. Wang, Z. Tang, L. Wang, H. Yang, W. Yan, S. Chen, Morphology control and electro catalytic activity towards oxygen reduction of peptide-templated metal nanomaterials: a comparison between Au and Pt, ChemistrySelect 1 (2016) 6044–6052.
[42] M. Hoefling, F. Iori, S. Corni, K.-E. Gottschalk, Interaction of amino acids with the Au(111) surface: adsorption free energies from molecular dynamics simulations, Langmuir 26 (2010) 8347–8351.
[43] J.A. Creighton, D.G. Eadon, Ultraviolet-visible absorption spectra of the colloidal metallic elements, J. Chem. Soc. Faraday Trans. 87 (1991) 3881–3891.
[44] J. Feng, R.B. Pandey, R.J. Berry, B.L. Farmer, R.R. Naik, H. Heinz, Adsorption mechanism of single amino acid and surfactant molecules to Au {111} surfaces in aqueous solution: design rules for metal-binding molecules, Soft Matter 7 (2011) 2113–2120.
[45] S. Kondo, M. Nakamura, N. Maki, N. Hoshi, Active sites for the oxygen reduction reaction on the low and high index planes of palladium, J. Phys. Chem. C 113 (2009) 12625–12628.
[46] R. Coppage, J.M. Slocik, B.D. Briggs, A.I. Frenkel, R.R. Naik, M.R. Knecht, Determining peptide sequence effects that control the size, structure, and function of nanoparticles, ACS Nano 6 (2012) 1625–1636.
[47] C.P. Deming, R. Mercado, V. Gadiraju, S.W. Sweeney, M. Khan, S. Chen, Graphene quantum dots-supported palladium nanoparticles for efficient electrocatalytic reduction of oxygen in alkaline media, ACS Sustain. Chem. Eng. 3 (2015) 3315–3323.
[48] C.D. Wagner, W.M. Riggs, L.E. Davis, J.F. Moudler, G.E. Muilenberg, Handbook of X-ray Photoelectron Spectroscopy: a Referencce Book of Standard Data for Use in X-ray Photoelectron Spectroscopy, Perkin-Elmer Corp., Edern Prairie MN, 1979, p. 1979.
[49] C.P. Deming, A. Zhao, Y. Song, K. Liu, M.M. Khan, V.M. Yates, S. Chen, Alkyne-protected AuPd alloy nanoparticles for electrocatalytic reduction of oxygen, ChemElectroChem 2 (2015) 1719–1727.
[50] A.L. Rucker, T.P. Creamer, Polyproline II helical structure in protein unfolded states: lysine peptides revisited, Protein Sci. 11 (2002) 980–985.
[51] X. Ge, A. Sumboja, D. Wuu, T. An, B. Li, F.W.T. Goh, T.S.A. Hor, Y. Zong, Z. Liu, Oxygen reduction in alkaline media: from mechanisms to recent advances of catalysts, ACS Catal. 5 (2015) 4643–4667.
[52] M. Shao, J. Odell, M. Humbert, T. Yu, Y. Xia, Electrocatalysis on shape-controlled palladium nanocrystals: oxygen reduction reaction and formic acid oxidation, J. Phys. Chem. C 117 (2013) 4172–4180.
[53] R. Quinn, T.A. Dahl, B.A. Toseland, An evaluation of synthesis gas contaminants as methanol synthesis catalyst poisons, Appl. Catal. A 272 (2004) 61–68.
[54] F.J. Ibañez, F.P. Zamborini, Ozone- and thermally activated films of palladium monolayer-protected clusters for chemiresistive hydrogen sensing, Langmuir 22 (2006) 9789–9796.
[55] Y.H. Xue, L. Zhang, W.J. Zhou, S.H. Chan, Pd nanoparticles supported on PDDA-functionalized carbon black with enhanced ORR activity in alkaline medium, Int. J. Hydrogen Energy 39 (2014) 8449–8456.